Effect of thickness and boundary conditions on the behavior of viscoelastic layers in sliding contact with wavy profiles

Effect of thickness and boundary conditions on the behavior of viscoelastic layers in sliding contact with wavy profiles.

N. Menga,[1,*] L. Afferrante,[1] and G. Carbone[1,2,3,4]

[1]*Department of Mechanics, Mathematics and Management, Politecnico of Bari, V.le Japigia, 182, 70126, Bari, Italy*
[2]*CNR - Institute for Photonics and Nanotechnologies U.O.S. Bari, Physics Department "M. Merlin", via Amendola 173, 70126 Bari, Italy*
[3]*Imperial College London, Department of Mechanical Engineering*
[4]*Exhibition Road, London SW7 2AZ*

Abstract

In this work, the sliding contact of viscoelastic layers of finite thickness on rigid sinusoidal substrates is investigated. Two different configurations are considered: a free layer with a uniform pressure applied on the top, and a layer rigidly confined on the upper boundary.

It is shown that the thickness affects the contact behavior differently, depending on the boundary conditions. In particular, the confined layer exhibits increasing contact stiffness when the thickness is reduced, leading to higher loads for complete contact to occur. The free layer, instead, becomes more and more compliant as thickness is reduced.

We find that, in partial contact, the layer thickness and the boundary conditions play a very peculiar role on the frictional behavior. Interestingly, at low contact penetrations, the confined layer shows higher friction coefficients compared to the free layer case; whereas, the scenario is reversed at large contact penetrations. Furthermore, for the confined layers, a shift of the sliding speed related to the friction coefficient peak is reported as the contact penetration increases. However, once full contact is established, the friction coefficient has a unique behavior not depending on thickness of the layer and boundary conditions.

Keywords: Contact mechanics, viscoelasticity, friction, fracture mechanics

*Electronic address: [Correspondingauthor.]Email:nicola.menga@poliba.it,phonenumber: +390805962746

I. INTRODUCTION

Rubber-like materials have found increasing utilization in the last decades in many practical applications, such as tyres, seals, conveyor and power transmission belts. The growing interest in polymeric materials, strongly supported by industrial demands, has boosted the scientific effort in such field of materials. The demanding problem of an accurate modelling of the viscoelastic contact behavior has been addressed by analytical approaches [1–7], numerical sophisticated simulations [8–13] and experimental investigations [14–18]. One of the most common assumptions in contact mechanics is that the contact bodies can be well represented by semi-infinite solids. This idea holds true for a large class of contact mechanics problems, as confirmed by theoretical arguments and experimental evidences. For instance, in the case of Hertzian contacts, it can be shown that, if the dimension of the contact area is sufficiently small compared with the thickness of the elastic bodies, the contact quantities can be correctly predicted by modelling the bodies as half-spaces.

However, when dealing with contacts involving thin layers, where the contact characteristic length is comparable with the layer thickness, the half-space assumption fails and the semi-infinite model is no longer able to correctly address the contact problem. Moreover, in the case of viscoelastic materials employed in power transmission belts, seismic energy dissipation systems, tyres, just to enumerate a few examples, the amount of dissipated energy and, in turn, the tribological properties of the contact are indeed strongly affected by the thickness.

For this reason, here we extend the results obtained in Ref. [7] for a viscoelastic half-plane in sliding contact with a periodic wavy profile, to the case of viscoelastic layers. In particular, we focus on two different configurations: a viscoelastic layer rigidly confined on the upper boundary and a free layer uniformly loaded on the top.

Such apparently simplified contact configuration is a powerful tool to investigate more complicated contact configurations. Hence, the proposed solution can be exploited in multi-scale approaches (e.g. [19, 20]) to capture the features of the viscoelastic contact of real randomly rough surfaces, which are the main focus of interest in modern contact mechanics ([4, 5, 21–26].

Under the assumption of steady sliding and taking into account linearity and translational invariance, the contact problem can be mathematically formulated in terms of a Fredholm integral equation of the first kind. However, since the value and the position of the contact area are not known *a priori*, two additional conditions are required. Such conditions can be obtained by observing that the mode I stress intensity factor K_I at the trailing and leading edges of the contact must vanish [27–29].

II. THE PROBLEM FORMULATION

Fig. 1 shows the sliding contact between a slightly wavy rigid profile with amplitude Λ and wavelength λ, and a viscoelastic layer of thickness h. As already mentioned, two different configurations are considered: a *free layer* with a uniform pressure applied on the upper edge, and a *layer rigidly confined* on the top. The contact penetration Δ is defined as the distance between the mean line of the deformed viscoelastic layer and the crests of the sinusoidal substrate, whereas the layer interfacial displacement $v(x,t)$ is measured from the mean line of the deformed body, i.e. it is calculated as the difference between the local and averaged displacement of the layer at the interface. Furthermore, any kind of tangential

interaction at the contact interface is neglected, as well as large deformations effects (e.g. membrane stress stiffening), as we focus on slightly wavy profile (i.e. $\Lambda/\lambda \ll 1$).

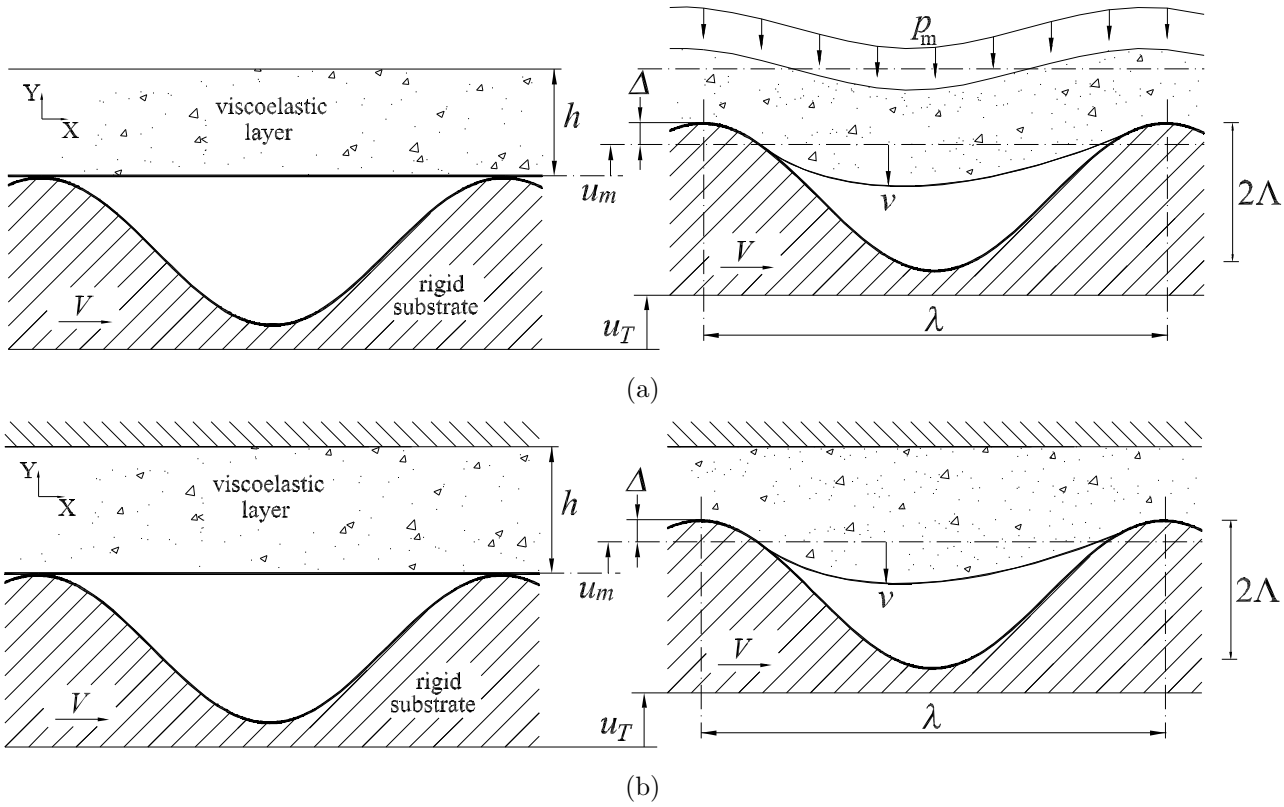

FIG. 1: The sliding contact of a viscoelasic layer of thickness h with a rigid slightly wavy profile. Different boundary conditions on the upper face are considered: (a) free layer (model A); (b) confined layer (model B). Tangential interactions at the interface are neglected. In particular, Δ is the contact penetration, and v is the layer displacement measured from the mean line of the deformed profile.

Under the assumption of steady sliding motion at constant velocity V, the layer displacement $v\left(x,t\right)$ and the contact pressure $p\left(x,t\right)$ are related, assuming linear viscoelasticity, through the equation [7, 8]

$$v\left(x\right) = -\int_{\Omega} \Theta_V\left(x-s\right) p\left(s\right) ds \tag{1}$$

where $\Omega = [-a, a]$ is the contact domain (see Fig. 2), and $\Theta_V\left(x\right)$ is the viscoelastic Green's function for steady sliding contacts, which parametrically depends on the sliding speed V. The function $\Theta_V\left(x\right)$ has been already derived for rolling contacts in Ref. [1], and for periodic contacts in Ref. [7], where it has been shown that

$$\Theta_V\left(x\right) = J\left(0^+\right) G\left(x\right) + \int_{0^+}^{+\infty} G\left(x+Vt\right) \dot{J}\left(t\right) dt \tag{2}$$

being $G\left(x\right)$ the '*purely elastic*' Green's function given in [17, 31], and $J\left(t\right)$ the viscoelastic creep function. The generalized linear viscoelastic model with a spring in series with N Voigt

elements (the latter consisting of a Hookean spring in parallel with a Newtonian dashpot) is usually employed to characterize $J(t)$. In such case

$$J(t) = \mathcal{H}(t) \left[\frac{1}{E_0} - \sum_{i=1}^{N} C_i \exp(-t/\tau_i) \right] \tag{3}$$

where $\mathcal{H}(t)$ is the Heaviside step function, E_0 is the zero-frequency elastic modulus of the material, τ_i are the relaxation times of the Voigt elements and C_i are the elastic compliances of the relative springs.

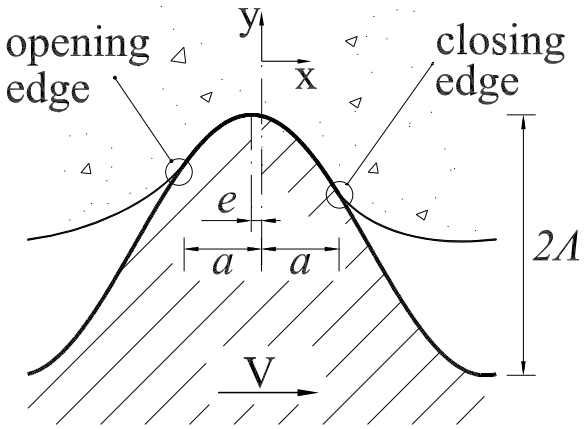

FIG. 2: The shape of the contact area. The contact area is shifted of a quantity e with respect to the crest of the sinusoidal asperity, because of the delay in the viscoelstic response of the material.

Substituting (3) in (2) and recalling that $J(+\infty) = 1/E_0$ and $J(0) = 1/E_\infty$, where E_∞ is the high frequency elastic modulus, the long time response viscoelastic Green's function writes as

$$\Theta_V(x) = \frac{1}{E_\infty} G(x) + \sum_{i=1}^{N} C_i \int_{0^+}^{+\infty} G(x + V\tau_i z_i) \exp(-z_i)\, dz_i \tag{4}$$

being $z_i = t/\tau_i$.

For a viscoelastic material with only one relaxation time, the creep function simplifies as

$$J(t) = H(t) \left[\frac{1}{E_0} - \frac{1}{E_1} \exp(-t/\tau) \right] \tag{5}$$

with $1/E_1 = 1/E_0 - 1/E_\infty$, and eq. (4) becomes

$$\Theta_V(x) = \frac{1}{E_\infty} G(x) + \frac{1}{E_1} \int_{0^+}^{+\infty} G(x + V\tau z) \exp(-z)\, dz \tag{6}$$

The expressions of the elastic Green's function $G(x)$ for both the models under investigation (see Fig. 1) can be given in the form (see Ref. [17, 31])

$$G(x) = \frac{2(1-\nu^2)}{\pi} \left(\log \left[2 \left| \sin\left(\frac{kx}{2}\right) \right| \right] + \sum_{m=1}^{\infty} A_m(kh) \frac{\cos(mkx)}{m} \right) \tag{7}$$

where $k = 2\pi/\lambda$ and

$$A_m\left(kh\right) = \frac{2mkh + \sinh\left(2mkh\right)}{1 + 2\left(mkh\right)^2 - \cosh\left(2mkh\right)} + 1 \tag{8}$$

for the free layer (Fig. 1a), and

$$A_m\left(kh\right) = \frac{2hkm - \left(3 - 4\nu\right)\sinh\left(2hkm\right)}{5 + 2\left(hkm\right)^2 - 4\nu\left(3 - 2\nu\right) + \left(3 - 4\nu\right)\cosh\left(2hkm\right)} + 1 \tag{9}$$

for the confined layer (Fig. 1b). Moreover, it can be shown that the displacement u_m of the mean plane is

$$u_{\mathrm{m}} = \frac{1+\nu}{1-\nu}\frac{1-2\nu}{E_0}p_{\mathrm{m}}h \tag{10}$$

where $p_{\mathrm{m}} = \lambda^{-1}\int_\Omega p\left(x\right)dx$ is the mean contact pressure.

A. Solution

Fig. 2 shows that the contact area is asymmetric with respect to the crest of the sinusoidal profile. In fact, due to the delay in the viscoelastic response of the material, the contact area presents a certain eccentricity e (see Ref. [7]). In the contact domain Ω, hence, where the layer displacement is $v\left(x\right) = \Delta - \Lambda\left[1 - \cos\left(kx + ke\right)\right]$, the Fredholm integral equation of the first kind (1) can be rewritten as

$$\Delta - \Lambda\left[1 - \cos\left(kx + ke\right)\right] = -\int_{-a}^{a}\Theta_V\left(x - s\right)p\left(s\right)ds \qquad x \in \Omega \tag{11}$$

Eq. (11) allows to calculate, for given Δ and V, the contact pressure distribution in terms of the contact size a and eccentricity e. In order to accomplish this purpose, we exploited the numerical procedure already drawn in Ref. [31], relying on nonuniform discretization of Ω. After calculating the contact pressure $p\left(x\right)$, the displacements in the region of non-contact can be evaluated as

$$v\left(x\right) = -\int_{-a}^{a}\Theta_V\left(x - s\right)p\left(s\right)ds \qquad x \notin \Omega \tag{12}$$

Anyway, in order to completely define the contact behavior, we need two additional conditions to calculate a and e. In this respect, according to [27–29], we can observe that the mode I stress intensity factors at the contact trailing and leading edges (see Fig. 2) must vanish. Therefore, recalling the expressions of K_I given in Ref. [32], we have

$$K_{I,1} = -\lim_{x\to a^-}\sqrt{2\pi\left(a - x\right)}p\left(x\right) = 0 \tag{13}$$

at the leading edge and

$$K_{I,2} = -\lim_{x\to -a^+}\sqrt{2\pi\left(a + x\right)}p\left(x\right) = 0 \tag{14}$$

at the trailing edge.

The contact size and eccentricity calculation can be mathematically formalized as a constrained optimization problem with objective function defined as

$$F(a,e) = K_{I,1}^2(a,e) + K_{I,2}^2(a,e) \tag{15}$$

with constraints

$$a \geq 0, e \geq 0 \tag{16}$$

It is worth noticing that the solution of the problem Eqs. (15, 16) is unique. In fact, the objective function $F(a,e)$ is convex as well as the feasible domain $T = \{(a,e) \in \mathbb{R}^2 \mid a \geq 0, e \geq 0\}$. The optimization problem then belongs to the class of convex optimization problems for which, recalling that $F(a,e) \geq 0$, only one global minimum exists.

III. EXAMPLE RESULTS

Results are given in terms of the following dimensionless quantities: $\tilde{h} = kh$, $\tilde{a} = ka$, $\tilde{\Lambda} = k\Lambda$, $\zeta = kV\tau$ and $\tilde{p} = 2(1-\nu^2)p/(Ek\Lambda)$. Moreover, in all calculations we have assumed $E_\infty = 3E_0$ and Poisson's ratio $\nu = 0.5$ (i.e. incompressible material), so that $u_m = 0$.

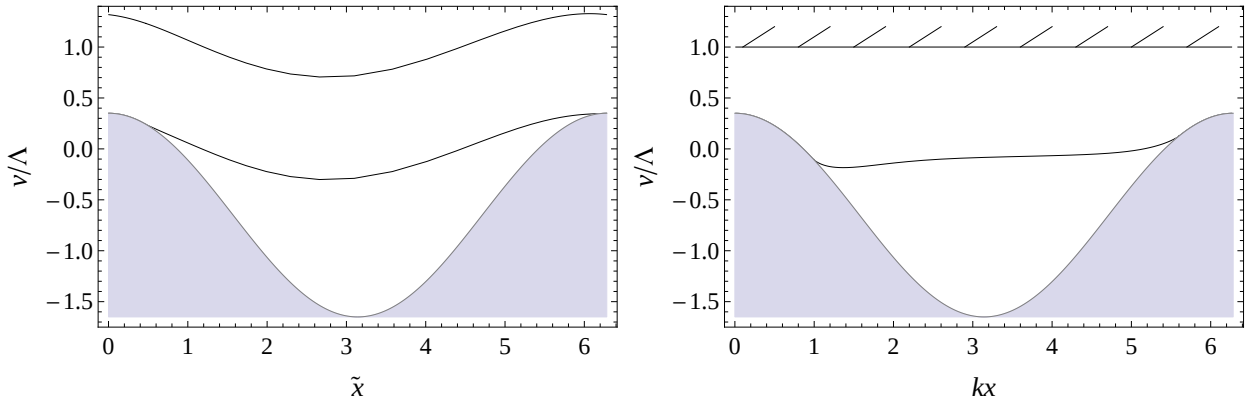

(a) (b)

FIG. 3: The dimensionless deformed profile of the free (a) and confined (b) layer. Results are obtained for $\tilde{h} = 1$, $\tilde{\Delta} = 0.35$, $\tilde{\Lambda} = 1$ and $\zeta = 1.5$. Notably, regardless of the configuration, both the contact area and the displacement field shows a certain asymmetry.

A. The contact behavior

Fig. 3 shows the deformed profile of the viscoelastic layer for both the models under investigation. Results are obtained under displacement controlled conditions, with $\Delta = 0.35$. In both cases, asymmetry in the displacement field and contact area occurs. Moreover, a smaller contact area is observed in the free layer model (Fig. 3a), as a result of a larger compliance.

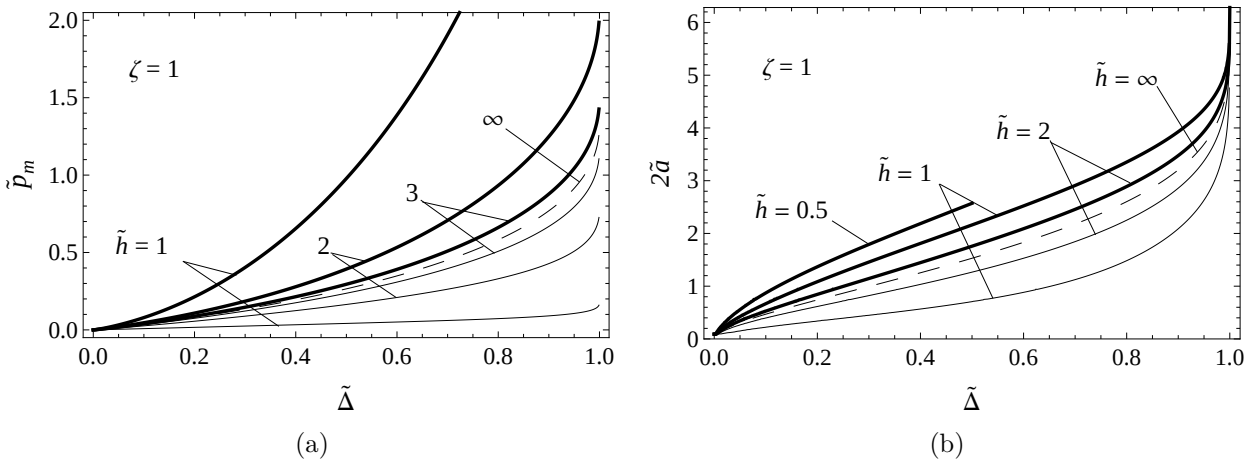

FIG. 4: The dimensionless mean contact pressure $\tilde{p}_m$ (a) and contact area $\tilde{a}$ (b) as functions of the dimensionless contact penetration $\tilde{\Delta}$ for different values of the dimensionless layer thickness $\tilde{h}$. Thick and thin solid lines refer, respectively, to the confined and to the free layer. The halfplane solution (given in Ref. [7]) is also plotted with dashed line. Results are given for $\tilde{\Lambda} = 1$ and $\zeta = 1$. In (b), complete contact is obtained when $\tilde{a} = \pi$.

The dimensionless mean contact pressure and contact area are plotted in Fig. 4 as functions of Δ, for fixed sliding velocity (we adopted $\zeta = 1$ to highlight the viscoelastic behavior) and different values of the layer thickness. Thin solid lines refer to the free layer, whereas thick solid lines are used for the confined layer. Notably, in the limit of $\tilde{h} \to \infty$, the viscoelastic half-plane solution [7] (dashed line) is recovered in both cases.

As expected (see Ref. [31, 33]), the thickness affects the contact behavior differently, depending on the layer boundary conditions. In fact, from Fig. 4a one infers that the free layer contact stiffness is reduced as the layer thickness increases, whereas the opposite behavior is observed for the confined layer. Moreover, Fig. 4b shows that the contact area of the confined layer (thicker lines) is larger compared to the viscoelastic half-plane case. Such a behavior can be related to the joint effect of material incompressibility and layer finite thickness (Ref. [31]). The free layer contact behavior (thinner curves), instead, is mainly governed by bending, as show in Ref. [33]. As a result, the contact area is very small and is negligibly affected by Δ at small contact penetrations, whereas a strong increase occurs when the penetration takes higher values, in proximity of the complete contact.

Fig. 5a shows, for $\tilde{h} = 1.5$, the influence of the sliding velocity on the minimum value of the mean contact pressure $\tilde{p}_{m,FC}$ required to obtain complete contact between the layer and the rigid substrate. The results are compared with the viscoelastic half-plane solution (given in Ref. [7]) and the viscoelastic Euler-Bernoulli (E-B) beam case (given in Appendix B).

Interestingly, we observe that the results are qualitatively similar in all the cases. In particular, at very low and very high sliding speeds the material behaves elastically, regardless of the system configuration. Moreover, in the intermediate range of ζ, the load required to establish full contact monotonically increases with the speed and, as expected, the ratio between the limiting values calculated at high and low velocities is equal to the ratio between the elastic moduli $E_\infty/E_0 = 3$. Even the trend of the increase of $\tilde{p}_{m,FC}$ is not affected by the

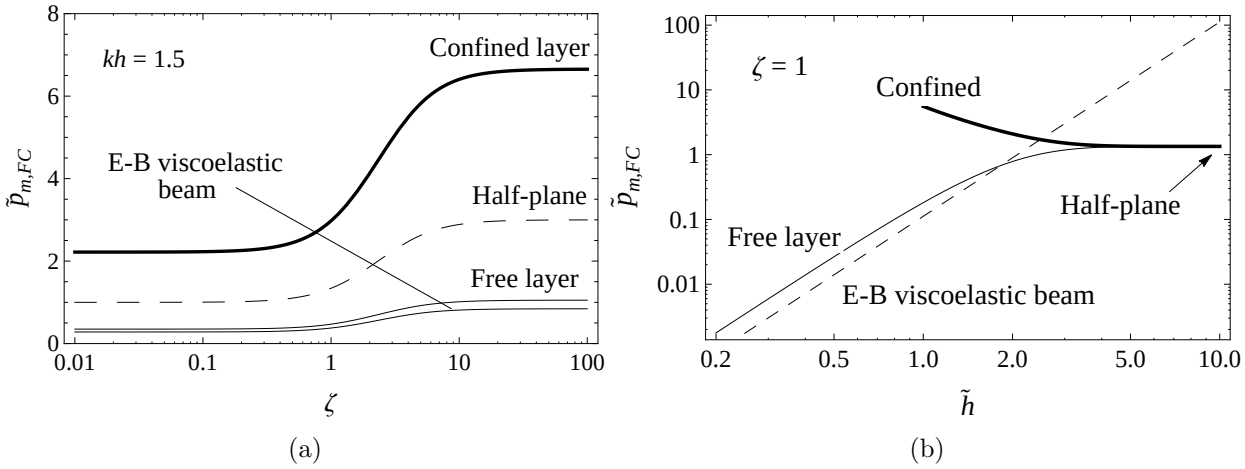

FIG. 5: The minimum value of the dimensionless mean pressure required to obtained full contact as a function of: (a) the dimensionless sliding velocity ζ, and (b) the dimensionless layer thickness $\tilde{h}$. Notice, the scales in the diagrams are different. The thin solid line refers to the free layer, whereas the thick line to the confined layer. The halfplane (dashed line) and the the Euler-Bernoulli viscoelastic beam (dashed-dot line) solutions are also plotted for comparison. Results are given for $\tilde{\Lambda} = 1$.

system configuration, hence the transition from the softer to the stiffer response occurs in the same range of ζ [see Eq. (A5) in Appendix A]. Finally, the observed results suggest that, applying a mean load lying in between the two limiting values of $\tilde{p}_{m,FC}$, a speed induced transition from full contact to partial contact can occur (see Ref. [7]).

Furthermore, $\tilde{p}_{m,FC}$ strongly depends on the layer thickness. This is clearly shown in Fig. 5b, where, at fixed $\zeta = 1$, the two configurations exhibit a very different behavior. Indeed, focusing on very thin free layers ($\tilde{h} \ll 1$), we observe that $\tilde{p}_{m,FC}$ vanishes. Additionally, the comparison with the viscoelastic E-B beam, which shows similar results in a relatively wide range of thickness ($0 < \tilde{h} < 2$), confirms that the free layer behavior is mainly related to a pure bending mode (see Ref. [33]). On the contrary, larger forces are required for the confined layer to achieve full contact, and a limiting thickness exists below which full contact can no longer be established because of the interference between the rigid profile and the upper rigid constraint. Again, for thicker layers, the differences between the two layer configurations vanish and, in the limit of $\tilde{h} \to \infty$, the viscoelastic half-plane solution is approached. Notably, for $\tilde{h} > 2$ the viscoelastic E-B beam model leads to unrealistic results.

B. The viscoelastic friction

Dealing with viscoelastic materials may, in general, give rise to global friction even when tangential interfacial stresses are neglected. This mechanism is strongly affected by the frequency spectrum of the external excitation: although the viscoelastic materials behave elastically for very low and very high frequencies, an intermediate range exists at which bulk energy dissipation and hence friction occurs [2]. Focusing on the problem under investigation, we expect that the boundary conditions and the thickness of the viscoelastic layer play a key role in determining the amount of energy dissipation. Firstly, notice that the stress and

strain fields in the bulk of the material are subjected to a spectrum of exciting frequencies, of which the fundamental is related to the substrate periodicity, thus being $\omega_0 = kV$. However, simple dimensional arguments show that the input spectrum must also present an important contribution at $\omega_a = 2\pi V/a = kV\,(\lambda/a)$, where a is the size of the contact area (depending on Δ). As we show in the sequel, the pulsating frequency ω_a has a fundamental role in determining the sliding velocity at which the systems exhibits the largest values of the viscoelastic friction coefficient.

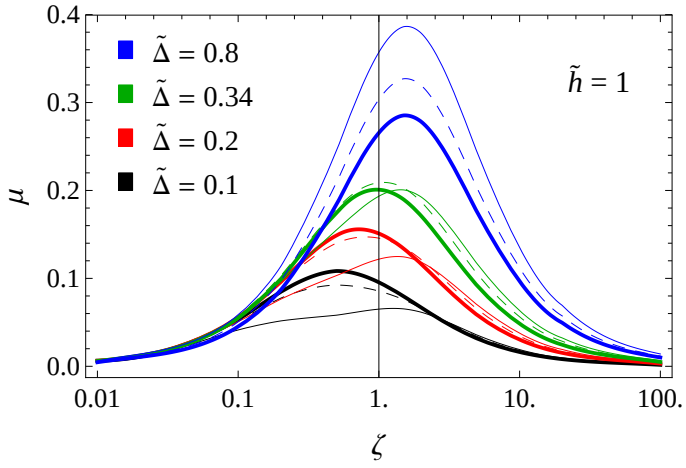

FIG. 6: The friction coefficient μ as a function of the dimensionless sliding velocity ζ for different dimensionless contact penetration $\tilde{\Delta}$. Results are given for $\tilde{h} = 1$ and $\tilde{\Lambda} = 1$. Thin solid lines refer to the free layer, whereas thick lines to the confined layer. The halfplane solution is also plotted with dashed line for comparison.

Let us consider first the free layer case. This contact configuration is characterized (for each given value of $\Delta < 1$) by a decrease of the contact area a as the thickness of the layer is reduced. This is clearly shown in Fig. 4b and can be easily explained in terms of local stiffness and bending stiffness of the layer (the reader is referred to Ref. [33] for a detailed explanation). Therefore, for thin layers, ω_a is large and must interest the glassy region of the viscoelastic spectrum of the material, where no dissipation and, hence, no friction is generated. In this case, the main contribution to viscoelastic friction comes from the fundamental frequency ω_0. Thus, the largest viscoelastic energy dissipation occurs when $\mathrm{Im}\left[E\left(\omega\right)\right]/\left|E\left(\omega\right)\right|$ is maximized, i.e. at values of $\omega_0\tau = kV\tau = \zeta \approx 1$ as, indeed, observed in Fig. 6 (thin lines).

The confined layer and the half-plane necessarily exhibit a significantly different behavior compared to the free layer case. In fact, this time, the quantity a, at given Δ, increases as the thickness of the layer is reduced (see Fig. 4b). Under this condition, an important contribution to energy dissipation, and hence to friction, occurs when $\omega_a\tau = kV\,(\lambda/a)\,\tau = \zeta\,(\lambda/a) \approx 1$, i.e., when $\zeta \approx a/\lambda < 1$. Increasing Δ from zero, leads to a continuous increase of the contact area a and, therefore, to an increase of the dimensionless velocity values ζ at which the friction peak is located. Finally, when Δ is close to 1, full contact conditions are almost established, i.e. $a \approx \lambda$, and the friction peak will be again obtained at $\zeta \approx 1$.

The above qualitative analysis is totally confirmed by the behavior shown in Fig. 6,

where the friction coefficient

$$\mu = -\frac{1}{p_{\mathrm{m}}\lambda}\int_{\Omega} p\left(x\right) v'\left(x\right) dx \tag{17}$$

is plotted as a function of the dimensionless sliding velocity ζ, for $\tilde{h} = 1$ and Δ ranging from small to high values. Bell-shaped curves are obtained in all cases, and vanishing friction occurs at high and low speeds.

Interestingly, dealing with large contact penetrations, the friction coefficient takes larger values for the free layer, whereas the opposite behavior is observed at small penetrations, where μ is larger for the confined layer and for the half-plane. The above results can be explained by arguing that, at large contact penetrations, the energy dissipation is large for the free layers, as the cyclic bending deformation involves the whole body. On the contrary, for confined layers and half-plane, bending is inhibited and the viscoelastic deformation involves regions of smaller size. In fact, given the penetration Δ, the deformation of the solid involves a volume (per unit width) of the order of a^2 (half-plane) or ah (confined layer, provided that $a \geq h$).

At small penetrations, if we focus on the contact region, the local penetration of the substrate into the layer can be estimated as $\delta_i \approx \Lambda\left[1 - \cos\left(ka_i\right)\right]$, where a_i is the contact area semi-width and $i = C, H, F$, where the subscripts C, H, and F refer, respectively, to the confined layer, the half-plane and the free layer. Moreover, since we deal with stationary conditions, the energy dissipated per unit width, when the contact advances of a distance λ, must balance the work done by the tangential force per unit width. Therefore, dimensional arguments lead to

$$F_T\lambda = E_d = \lambda\int_{\Omega} pu'\left(x\right) dx \approx \lambda p_{\max}\frac{\delta_i}{2a_i}\left(2a_i\right)\sin\left[\varphi\left(\omega\right)\right] = \lambda\delta_i p_{\max}\sin\left[\varphi\left(\omega\right)\right] \tag{18}$$

and

$$F_T \approx p_{\max}\delta_i\sin\left[\varphi\left(\omega\right)\right] \tag{19}$$

where $\varphi\left(\omega\right) = \arg[E\left(\omega\right)]$. Notice in the above estimation we have introduced the quantity $\sin\left[\varphi\left(\omega\right)\right]$ because, being the friction force due to the energy dissipation in the viscoelastic medium, F_T must be proportional to $\mathrm{Im}\left[E\left(\omega\right)\right] / \left|E\left(\omega\right)\right|$ (see appendix A and Ref. [34]).

The normal force per unit width is instead

$$F_N \approx p_{\max}\left(2a_i\right) \tag{20}$$

and

$$\mu_i = \frac{F_T}{F_N} \approx \frac{\delta_i}{2a_i}\sin\left[\varphi\left(\omega\right)\right] \tag{21}$$

Taking the ratio between the free layer and confined layer friction coefficients one gets

$$\frac{\left(\mu_F\right)_{\max}}{\left(\mu_C\right)_{\max}} \approx \frac{\delta_F}{a_F}\frac{a_C}{\delta_C} \tag{22}$$

which for small contact areas, i.e. $\Delta \ll 1$, being $\delta_i \approx \Lambda\left(ka_i\right)^2/2$, gives

$$\frac{\left(\mu_F\right)_{\max}}{\left(\mu_C\right)_{\max}} \approx \frac{a_F}{a_C} < 1 \tag{23}$$

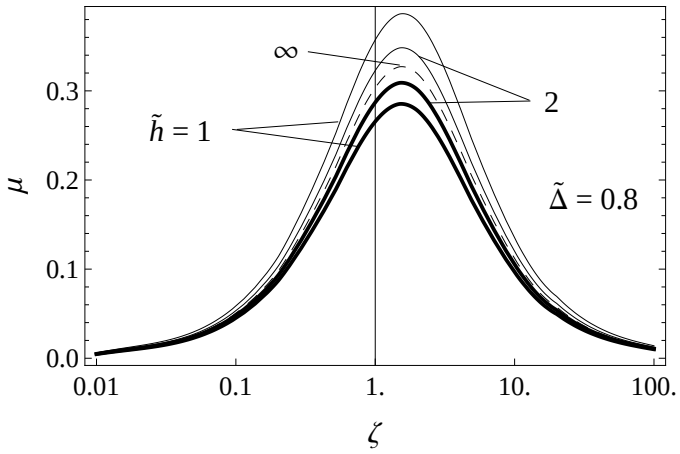

FIG. 7: The friction coefficient μ as a function of the dimensionless sliding velocity ζ for different dimensionless values of the thickness $\tilde{h}$, $\tilde{\Delta} = 0.8$ and $\tilde{\Lambda} = 1$. Thin solid lines refer to the free layer, whereas thick lines to the confined layer. The halfplane solution is also plotted with dashed line for comparison. The free layers show higher friction coefficient, compared to the confined ones.

as, from Fig. 4b, $a_F < a_C$.

Finally, Fig. 7, shows the effect of thickness on the friction coefficient, for a given ζ. The half-plane solution (dashed curve) is recovered for increasing values of $\tilde{h}$. We note, however, that the effect of thickness on the friction curves must vanish when complete contact conditions are considered. In fact, as shown in appendix A, full contact friction only depends on the dimensionless amplitude $k\Lambda$ of the wavy profile and on the argument of the complex viscoelastic modulus of the material.

IV. CONCLUSIONS

In this paper, the sliding contact of a viscoelastic layer on a rigid sinusoidal profile is analyzed. In particular, we have focused on two different system configurations: a free layer loaded with a uniform pressure on the upper boundary, and a layer rigidly constrained on the top. As expected, the latter shows higher contact stiffness that is reduced by increasing the layer thickness h. An opposite trend is exhibited by the free layer. Anyway, the differences in the behavior of the two configurations vanish as the layer thickness increases, finally leading to the half-plane solution in both cases.

As typical in viscoelasticity, different behaviors can be identified depending on the sliding speed: at low and high sliding speeds, the system behaves elastically and the corresponding pressures required to obtained complete contact are related by the proportionality factor E_∞/E_0 ; at intermediate speeds, viscous effects are dominant and a threshold speed can be defined, above which, under load controlled conditions, a transition from full contact to partial contact occurs.

Since the hysteretic behavior of viscoelastic materials gives rise to global friction also in absence of tangential interfacial stresses, the dependence of the friction coefficient μ on the sliding speed has been investigated. At high contact penetrations, the free layer shows higher values of μ, as larger amount of material is involved in cyclic deformations, giving

rise to higher dissipation compared to the confined layer. At low contact penetrations, the opposite behavior is observed accompanied, in the case of confined layer, by a shifting of the sliding speed at which the friction peak occurs. We qualitatively estimate these results by means of dimensional arguments.

Finally, in the Appendix, we show that the friction coefficient, in full contact conditions, is not affected by the layer configuration, and only depends on the amplitude of the sinusoidal profile and on the complex elastic modulus.

APPENDIX A: FRICTION FOR A VISCOELASTIC LAYER IN FULL CONTACT WITH A SINUSOIDAL PROFILE

In what follows, we consider a viscoelastic layer in full contact with a rigid sinusoidal profile. Because of the linearity of the problem, in the Fourier domain, the stress σ and the displacement v are related by (see, for example, Ref. [4, 17])

$$\sigma\left(k,\omega\right)=M^{-1}\left(k,\omega,h\right)v\left(k,\omega\right) \tag{A1}$$

where

$$\sigma\left(k,\omega\right)=\int dxdt\sigma\left(x,t\right)e^{-i(kx-\omega t)} \tag{A2}$$

$$v\left(k,\omega\right)=\int dxdtv\left(x,t\right)e^{-i(kx-\omega t)} \tag{A3}$$

and

$$M\left(k,\omega,h\right)=\frac{G\left(k,h\right)}{E\left(\omega\right)} \tag{A4}$$

is the viscoelastic response function, and G is a function accounting for the periodicity of the contact and the thickness of the layer. The sinusoidal profile is $v\left(x\right)=\Lambda\cos\left(kx\right)$. At constant sliding velocity V, the displacements field and the interfacial stress distribution will have different phases. Moreover, the viscoelastic material is subjected to a single exciting frequency $\omega=kV$. As a result, since the system is linear, the stress at the interface can be written as

$$\sigma\left(x\right)=\sigma_0\left[1+\cos\left(kx+\varphi\right)\right]$$

where

$$\sigma_0=\Lambda\left|M^{-1}\left(k,kV,h\right)\right| \tag{A5}$$

$$\begin{aligned}\varphi&=\arg\left[M^{-1}\left(k,kV,h\right)\right]\\&=\arg\left[E\left(kV\right)\right]\end{aligned} \tag{A6}$$

The friction force due to the viscoelastic dissipation is then

$$F_T=\int_\lambda dx\sigma(x,kV)v'\left(x\right) \tag{A7}$$

$$=\pi\Lambda^2\left|M^{-1}\left(k,kV,h\right)\right|\sin\left(\varphi\right) \tag{A8}$$

$$=\pi\Lambda^2\Im\left[M^{-1}\left(k,kV,h\right)\right] \tag{A9}$$

where $\lambda = 2\pi/k$. Now, recalling that $F_N = \lambda\sigma_0$, the friction coefficient is then

$$\mu = \frac{F_T}{F_N} = \frac{k\Lambda \sin\left[\arg\left[E\left(kV\right)\right]\right]}{2} \tag{A10}$$

which is identical to that obtained in Ref. [7] dealing with a viscoelastic half-plane.

Eq. (A10) shows that, in the case of full contact with a sinusoidal profile, the main contact quantities, as well as the friction coefficient, are not affected by the layer thickness, and only depend on the amplitude Λ of the wavy profile and on the viscoelastic material response $E\left(\omega\right)$. Hence, it follows that, under these conditions, even the trends of the σ_0 and μ with respect to the sliding speed V are the same regardless of the system configuration, as V only affects $E\left(\omega = kV\right)$.

APPENDIX B: THE 2D EULER-BERNOULLI VISCOELASTIC BEAM RESPONSE FUNCTION

The equilibrium equation for a 2D Euler-Bernoulli elastic beam is

$$u^{IV}\left(x,t\right) = \frac{\sigma\left(x,t\right)}{EI} \tag{B1}$$

where u^{IV} is the fourth spatial derivative of the displacement field, E is the elastic modulus, and I is the second moment of area of the beam cross-section.

For a viscoelastic beam, on the basis of the elastic-viscoelastic correspondence principle, eq. (B1) can be rewritten in the Fourier domain as

$$u\left(k,\omega\right) = \frac{\sigma\left(k,\omega\right)}{k^4 E\left(\omega\right) I} \tag{B2}$$

Therefore, referring to Eq. (A1), the response function of a 2D Euler-Bernoulli viscoelastic beam is

$$M\left(k,\omega\right) = \frac{1}{k^4 E\left(\omega\right) I} \tag{B3}$$

[1] Hunter S.C. , The rolling contact of a rigid cylinder with a viscoelastic half space Trans. ASME, Ser. E, J. Appl. Mech. 28, 611–617, 1961.

[2] Grosch K. A. , The Relation between the Friction and Visco-Elastic Properties of Rubber, Proceedings of the Royal Society of London. Series A, Mathematical and Physical, 274-1356, 21-39, 1963.

[3] Panek C. and Kalker J.J., Three-dimensional Contact of a Rigid Roller Traversing a Viscoelastic Half Space, J. Inst. Maths Applies 26, 299-313, 1980.

[4] Persson B.N.J.,Theory of rubber friction and contact mechanics, Journal of Chemical Physics, 115, 3840 -3861, 2001.

[5] Persson B.N.J., Rolling friction for hard cylinder and sphere on viscoelastic solid, Eur. Phys. J. E, 33, 327-333, 2010.

[6] M. Harrass, K.Friedrich , A.A.Almajid,Tribological behavior of selected engineering polymers under rolling contact, Tribology International, 43, 635–646, 2010.

[7] Menga N, Putignano C, Carbone G, Demelio GP. 2014 The sliding contact of a rigid wavy surface with a viscoelastic half-space. Proc. R. Soc. A, 470, 20140392, 2014.
[8] Carbone G. and Putignano C., A novel methodology to predict sliding and rolling friction of viscoelastic materials, Theory and experiments, J. of Mech. and Phys. Solids, 61, 1822-1834, 2013.
[9] Padovan J., O. Paramadilok, Transient and steady state viscoelastic rolling contact, Comput Struct, 20, 545-553, 1984.
[10] Padovan J., Finite element analysis of steady and transiently moving/rolling nonlinear viscoelastic structure-I. theory. Computers & Structures, 27(2):249–257, 1987.
[11] Padovan J., Kazempour A., Tabaddor F. and Brockman B., Alternative formulations of rolling contact problems. Finite Elements in Analysis and Design, 11:275–284, 1992.
[12] L. Nasdala, M. Kaliske, A. Becker, H. Rothert, An efficient viscoelastic formulation for steady-state rolling structures, Computational Mechanics 22, 395-403, 1998.
[13] Le Tallec P., Rahler C., Numerical models of steady rolling for non-linear viscoelastic structures in finite deformations, International Journal for Numerical Methods in Engineering, 37, 1159-1186, 1994.
[14] Schapery R.A., On the characterization of nonlinear viscoelastic materials, Polymer Engineering & Science, 9(4), 295-310, 1969.
[15] Faisca R.G, Magluta C. and Roitman N., Experimental Characterization of Viscoelastic Materials as Vibration Dampers, Journal of Engineering Mechanics, 127(9), 959-962, 2001.
[16] Odegard G.M., Gates T.S. and Herring H.M., Characterization of viscoelastic properties of polymeric materials through nanoindentation, Experimental Mechanics, 45(2), 130-136, 2005.
[17] Carbone G., Lorenz B., Persson B.N.J. and Wohlers A., Contact mechanics and rubber friction for randomly rough surfaces with anisotropic statistical properties, The European Physiscal Journal E – Soft Matter, 29(3), 275–284, 2009.
[18] Martina D., Creton C., Damman P., Jeusette M. and Lindner A., Adhesion of soft viscoelastic adhesives on periodic rough surfaces, Soft Matter 8(19), 5350-5357, 2012.
[19] Ciavarella M., Demelio G., Barber J.R. and Jang Y. H., Linear elastic contact of the Weierstrass profile, Proc. R. Soc. A, 456, 387-405, 2000.
[20] Afferrante L. Ciavarella M. and Demelio G., Adhesive contact of the Weierstrass profile, Proc. R. Soc. A, 471: 20150248, 2015 (doi: 10.1098/rspa.2015.0248).
[21] Persson B.N.J., Rubber friction: role of the flash temperature, J. Phys. Condensed Matter, 18(32), 7789–7823, 2006.
[22] Campana C., Mueser M.H. and Robbins M.O., Elastic contact between self-affine surfaces: comparison of numerical stress and contact correlation functions with analytic predictions. J. Phys. Condens. Matter, 20(35), 354013, 2008.
[23] Campana C., Persson B.N.J. and Mueser M.H., Transverse and normal interfacial stiffness of solids with randomly rough surfaces. J. Phys. Condens. Matter, 23 (8), 085001, 2011.
[24] Putignano C., Afferrante L., Carbone G. and Demelio G., A new efficient numerical method for contact mechanics of rough surfaces. Int. J. Solids Struct., 49(2),338–343, 2012.
[25] Afferrante L., Carbone G. and Demelio G., Interacting and coalescing Hertzian asperities: a new multiasperity contact model. Wear, 278-279, 28-33, 2012.
[26] Putignano C., Afferrante L., Carbone G. and Demelio G., A multiscale analysis of elastic contacts and percolation threshold for numerically generated and real rough surfaces, Tribology International, 64, 148-154, 2013.
[27] Charmet, J.C., Barquins, M., 1996. Adhesive contact and rolling of a rigid cylinder under the

pull of gravity on the underside of a smooth-surfaced sheet of rubber. Int. J. Adhes. 16 (4), 249–254.

[28] Shull, K.R., 2002. Contact mechanics and the adhesion of soft solids. Mater. Sci. Eng. R — Rep. 36 (1), 1–45.

[29] Carbone G., Mangialardi L., Adhesion and friction of an elastic half-space in contact with a slightly wavy rigid surface, Journal of the Mechanics and Physics of Solids, 52(6), 1267-1287, 2004.

[30] Christensen R. M., Theory of viscoelasticity, Academic Press, New York, 1982.

[31] Carbone G., Mangialardi L.: Analysis of adhesive contact of confined layers by using a Green's function approach, The Journal of the Mechanics and Physics of Solids, 56(2), 684-706, 2008.

[32] Maugis, D., Contact Adhesion and Rupture of Elastic Solids. Springer-Verlag Berlin Heidelberg, 2000.

[33] Menga N., Afferrante L. and Carbone G., Adhesive and adhesiveless contact mechanics of elastic layers on slightly wavy rigid substrates, Int. J. Solids Struct., accepted, 2016.

[34] Persson B.N.J., Sliding Friction, Springer-Verlag Berlin Heidelberg, 2000.